

## RADIATING BONDI AND COOLING SITE FLOWS

WILLIAM G. MATHEWS<sup>1</sup> AND FULAI GUO<sup>1</sup>

*Draft version September 26, 2018*

### ABSTRACT

Steady accretion of a radiating gas onto a central mass point is described and compared to classic Bondi accretion. Radiation losses are essential for accretion flows to be observed. Unlike Bondi flows, radiating Bondi flows pass through a sonic point at a finite radius and become supersonic near the center. The morphology of all radiating flows is described by a single dimensionless parameter proportional to  $\dot{M}/MT_s$  where  $T_s$  is the gas temperature at the sonic point. In radiating Bondi flows the relationship between the mass accretion rate and central mass,  $\dot{M} \propto M^p$  with  $p \sim 1$ , differs significantly from the quadratic dependence in classical Bondi flows,  $\dot{M} \propto M^2$ . Mass accretion rates onto galaxy or cluster-centered black holes estimated from traditional and radiating Bondi flows are significantly different. In radiating Bondi flows the gas temperature increases at large radii, as in the cores of many galaxy groups and clusters, allowing radiating Bondi flows to merge naturally with gas arriving from their cluster environments. Some radiating flows cool completely before reaching the center of the flow, and this also occurs in cooling site flows, in which there is no central gravitating mass.

*Subject headings:* hydrodynamics, galaxies: cooling flows, galaxies: clusters

### 1. INTRODUCTION

Bondi flow describes the steady spherical inflow of an adiabatic gas toward an accreting mass point. As gas flows radially toward the gravitating mass, its density increases due to tidal compression by the gravity field and consequently its temperature also increases. Gas at rest at infinity with uniform temperature and density accelerates steadily as it flows inward toward the central mass. In Bondi flow the mass of flowing gas is assumed to be small so its self-gravity can be neglected and the central mass can be regarded as constant during relevant flow times (Bondi 1952). Conventional non-radiating Bondi flows are often used in computational studies of massive black hole growth during galaxy formation or to detect errors in hydrocodes. Bondi flows are also often used to estimate black hole accretion rates from X-ray observations of gas near central black holes in galaxies and galaxy clusters. However, Bondi flows do not radiate.

For more realistic astrophysical applications, such as the flow of hot intracluster gas toward a cluster-centered black hole, the gas must radiate as it flows inward. Our purpose here is to illustrate that steady spherical accretion flow solutions with radiative losses differ fundamentally from the traditional Bondi solution. A large family of morphologically varied radiating solutions are possible, all characterized by a single dimensionless parameter. But the most important difference is that the often-assumed quadratic Bondi relation between the mass accretion rate and the central mass,  $\dot{M} \propto M^2$ , no longer holds. Instead, radiating flows require  $\dot{M} \propto M^p$  with  $p \sim 1$ . Unlike classical Bondi flow, the gas temperature in radiating solutions always increases at large radii, allowing more natural fits to the hot gas cores in galaxy groups and clusters that also have positive temperature

gradients. Radiating Bondi flows can also accommodate larger accretion rates  $\dot{M}$  due to gas flowing in from an extended cluster environment.

To be useful in cosmological evolutionary computations and in interpreting accretion rates from X-ray observations, it is useful to keep our solutions as simple and general as possible. Consequently, our radiating steady solutions do not include spatially distributed mass of stars or dark matter (e.g. Yahil & Ostriker 1973; Cowie & Binney 1977; Fabian & Nulsen 1977; Mathews & Bregman 1978; Quataert & Narayan 2000; Guo, Oh, & Ruszkowski 2008), feedback energy, or rotation (Park 2009; Brighenti et al. 2009; Narayan & Fabian 2011).

When radiative losses are included, an initially hot gas can sometimes cool to zero temperature before it reaches the concentrated mass at the center, particularly if the central mass is sufficiently small or if there is no central gravitating mass at all. This latter type of flow toward a cooling site in the absence of gravity experiences no tidal compression so the gas temperature decreases continuously toward the origin, becoming supersonic before cooling to zero temperature. Cooling site flows may describe the appearance and evolution of cool, non-central low-entropy gas often observed in galaxy clusters far from the gravitating cluster core.

### 2. FLOW EQUATIONS

Consider the equations for steady spherical Bondi accretion toward a point mass  $M$  but also include optically thin radiative losses:

$$\dot{M} = \rho u 4\pi r^2 \quad (1)$$

$$\rho u \frac{du}{dr} = -\frac{dP}{dr} - \rho \frac{GM}{r^2} \quad (2)$$

and

$$\rho u \frac{d\varepsilon}{dr} = \frac{P}{\rho} u \frac{d\rho}{dr} - \left( \frac{\rho}{m_p} \right)^2 \Lambda. \quad (3)$$

<sup>1</sup> University of California Observatories/Lick Observatory, Department of Astronomy and Astrophysics, University of California, Santa Cruz, CA 95064 mathews@ucolick.org

The mass flow  $\dot{M}$  is negative for inflowing gas,  $u < 0$ . The specific thermal energy  $\varepsilon = (P/\rho)/(\gamma - 1) = 3P/2\rho$  with  $\gamma = 5/3$ . For simplicity we assume that the optically thin cooling coefficient  $\Lambda$  (erg cm<sup>3</sup> s<sup>-1</sup>) is constant throughout the flow. While the temperature dependence of  $\Lambda$  is well-known (e.g. Sutherland & Dopita 1993), the quadratic density coefficient in the cooling term contributes much more to the non-linear cooling process than the comparatively slower variation of  $\Lambda$  with temperature. Moreover, a constant  $\Lambda$  is easy to implement in checking gasdynamical hydrocodes.

The three flow equations can be reduced to two by eliminating the density  $\rho$  using equation (1):

$$\frac{du}{dr} = \frac{u}{r(3u^2 - 5\theta)} \left[ 10\theta - 3\frac{GM}{r} + \frac{2\lambda}{u^2 r} \right] \quad (4)$$

$$\frac{d\theta}{dr} = \frac{\theta}{r(3u^2 - 5\theta)} \left[ -4u^2 + 2\frac{GM}{r} + \left( 1 - \frac{u^2}{\theta} \right) \frac{2\lambda}{u^2 r} \right] \quad (5)$$

where

$$\lambda = \frac{\dot{M}\Lambda}{4\pi m_p^2}. \quad (6)$$

and

$$P = \rho\theta \quad \text{where} \quad \theta = \frac{kT}{\mu m_p} \quad \text{so} \quad \varepsilon = \frac{3}{2}\theta. \quad (7)$$

These equations become singular at the sonic radius  $r = r_s$  where the flow speed equals the local adiabatic sound speed,

$$u_s = c_s = (5\theta_s/3)^{1/2}. \quad (8)$$

The sonic radius is found by insisting that both square brackets in the equations above vanish when  $u = (5\theta/3)^{1/2}$ , i.e.

$$r_s = \frac{15\theta_s GM - 6\lambda}{50\theta_s^2}. \quad (9)$$

Use of L'Hôpital's rule on the right side of either equation (4) or (5) at the sonic point singularity gives the following logarithmic slopes at the sonic radius (subscript  $s$ )

$$\left( \frac{d \log u}{d \log r} \right)_s = \frac{1}{2} [-b \pm (b^2 - 4c)^{1/2}] \quad (10)$$

$$\left( \frac{d \log \theta}{d \log r} \right)_s = -\frac{2}{3} \left[ 2 + \frac{3\lambda}{5\theta_s^2 r_s} + \left( \frac{d \log u}{d \log r} \right)_s \right] \quad (11)$$

where

$$b = 1 + \frac{33}{100} \frac{\lambda}{\theta_s^2 r_s} \quad \text{and} \quad c = 1 + \frac{39}{100} \frac{\lambda}{\theta_s^2 r_s} - \frac{9}{40} \frac{GM}{\theta_s r_s}. \quad (12)$$

Beginning at the sonic point, equations (4) and (5) can be integrated inward and outward using the sonic slopes in equations (10) and (11). The sign option in equation (10) can be chosen for inflow or outflow. We restrict our discussion here to inflow solutions (minus sign).

The structure of solutions of equations (4) and (5) is more apparent when transformed to dimensionless variables

$$\xi = \frac{r}{r_s} \quad \eta = \frac{u^2}{u_s^2} \quad \tau = \frac{\theta}{\theta_s} \quad (13)$$

in which the differential equations become

$$\frac{d\eta}{d\xi} = \frac{2\eta}{\xi(\eta - \tau)} \left[ 2\tau - \frac{30}{A} \frac{1}{\xi} + \frac{12a}{A} \frac{1}{\eta\xi} \right] \quad (14)$$

$$\frac{d\tau}{d\xi} = \frac{\tau}{\xi(\eta - \tau)} \left[ -\frac{4}{3}\eta + \frac{20}{A} \frac{1}{\xi} + \left( 1 - \frac{5}{3} \frac{\eta}{\tau} \right) \frac{12a}{A} \frac{1}{\eta\xi} \right] \quad (15)$$

where  $A = (15 - 6a)$  and

$$a = \frac{1}{4\pi m_p^2} \frac{\Lambda \dot{M}}{GM} \frac{5}{3c_s^2}. \quad (16)$$

It is remarkable that the morphology of all flow solutions  $\eta(\xi)$  and  $\tau(\xi)$  depends on only one dimensionless parameter

$$a = 0.1008 \frac{(\dot{M}/M_\odot \text{ yr}^{-1})(\Lambda/10^{-23} \text{ erg cm}^3 \text{ s}^{-1})}{(T_s/10^7 \text{ K})(M/10^9 M_\odot)} \quad (17)$$

where  $\mu = 0.61$ . Since  $\dot{M} < 0$ ,  $a$  must also be negative or zero and we consider values in the range  $-\infty < a \leq 0$ .

When radiative cooling is small,  $\Lambda \rightarrow 0$ , both  $a$  and  $\lambda$  also become small and equations (4) and (5) describe standard adiabatic Bondi flow. When  $\gamma = 5/3$ , which we consider here, the traditional non-radiating Bondi accretion solution is unique, entirely subsonic and singular since the sonic point lies exactly at the origin,  $r_s = 0$ . Since our dimensionless variable  $\xi = r/r_s$  is inappropriate when  $r_s = 0$ , we do not discuss the transition to standard adiabatic flow in detail here. When the central mass is small,  $a \rightarrow -\infty$ , solutions approach mass-free flow toward a cooling site with  $M = 0$ . For sufficiently large  $|a|$  inflowing gas can cool completely ( $\theta \rightarrow 0$ ) before reaching the origin.

### 3. RADIATING BONDI FLOWS

The top and central panels of Figure 1 show eight superposed solutions of equations (14) and (15),  $\eta(\xi)$  and  $\tau(\xi)$ , each corresponding to a different value of the parameter  $|a| = 10^{-6}, 10^{-2}, 0.1, 1, 1.5, 3, 10$  and 100. The dotted extensions toward the left for each of these solutions describe supersonic flow within the sonic radius  $\xi < 1$ . The dimensionless temperature  $\tau = \theta/\theta_s$ , shown in the central panel of Figure 1, has the largest variation with  $|a|$ . For  $|a| \geq 3$  all plotted flows cool monotonically to zero temperature at a finite radius  $\xi_{cool}$  not far within the sonic radius. At zero temperature the cooled gas would go into free fall toward the central mass, but this is not explicitly calculated.

The parameter  $a$  is related to ratios between the flow, free fall and cooling times

$$\frac{t_{ff}}{t_{flow}} = \frac{\pi}{4} \alpha^{1/2} \quad \frac{t_{flow}}{t_{cool}} = \frac{4}{3} \frac{|a|}{\alpha} \quad \frac{t_{ff}}{t_{fcool}} = \frac{\pi}{3} \frac{|a|}{\alpha^{1/2}}$$

where  $\alpha = 1 + (2/5)|a|$  and the times

$$t_{flow} = \frac{r_s}{u_s} \quad t_{ff} = \frac{\pi}{2} \frac{r_s^{3/2}}{(2GM)^{1/2}} \quad t_{cool} = \frac{\varepsilon_s m_p^2}{\Lambda \rho_s}$$

are evaluated at the sonic radius  $r_s$ .

The dimensionless velocity variable  $\eta(\xi) = u^2/u_s^2$  decreases monotonically with radius for all radiatively cooling solutions. For  $|a| \leq 10^{-6}$  the top panel in Figure 1

shows that the velocity variable  $\eta(\xi)$  is nearly a single power law but becomes a double power law for  $|a| \gtrsim 0.1$ , broken at the sonic radius  $\xi = 1$ .

Of particular interest are radiating flows with  $|a| \gtrsim 3$  in which the gas temperature drops to zero before it reaches the flow center. These solutions are expected when the central mass  $M$  (and/or the sonic point temperature  $T_s$ ) becomes sufficiently small or when  $\dot{M}$  is unusually large. When  $|a| \geq 1$ , the overlapping dotted lines for  $\eta(\xi)$  in Figure 1 obscure the different leftward terminations of  $\eta(\xi)$  which do not extend within the radius  $\xi_{cool}$  where  $\tau \rightarrow 0$  in the bottom panel, with  $\xi_{cool}$  increasing with  $|a|$ .

A temperature minimum at  $\xi = \xi_{min}$  characteristic of radiating Bondi flows having smaller  $|a|$  appears in Figure 1 for the first time at  $\log \xi_{min} \approx -1$  in the supersonic flow for  $|a| = 1.5$ . As  $|a|$  decreases further, the location  $\xi_{min}$  of the minimum in  $\tau(\xi)$  moves progressively toward larger radii:  $\log \xi_{min} \approx -0.1, 0.6,$  and  $1.4$  for  $|a| = 1, 0.1$  and  $0.01$  respectively. For  $|a| \leq 10^{-6}$  the temperature minimum has moved to  $\log \xi > 2$  and no longer appears in Figure 1. For these very small values of  $|a|$  the profiles for both  $\eta(\xi)$  and  $\tau(\xi)$  converge to power laws in  $\xi \lesssim 100$  that appear as single straight lines in the region plotted in Figure 1.

Using equation (1), the corresponding dimensionless gas density variable

$$\delta = \frac{\rho}{\rho_s} = \frac{1}{\eta^{1/2} \xi^2} \quad (18)$$

is normalized with the gas density at the sonic radius  $\rho_s$ . The bottom panel in Figure 1 shows that  $\delta(\xi)$  decreases monotonically with radius for all solutions.

The flow profiles in Figure 1 for velocity, temperature and density in dimensionless variables have morphologies that depend only on the single dimensionless parameter  $|a|$ . However, when these results are converted into physical units, (two of) the fundamental dimensional flow parameters in equation (16) –  $M$ ,  $\dot{M}$ ,  $T_s$  and  $a$  – become individually important, particularly for the normalizing factors  $r_s$  and  $\rho_s$ . The sonic radius

$$r_s = \frac{(15 - 6a) GM}{50 \theta_s} \quad (19)$$

depends on  $GM/\theta_s$  as well as  $a$  and the density at the sonic radius

$$\rho_s = -\frac{\dot{M}}{4\pi r_s^2} \left( \frac{3}{5\theta_s} \right)^{1/2} \quad (20)$$

has its own unique dependence on flow parameters.

All flows with  $|a| \lesssim 3$  have a central thermal peak. It is of interest to consider the total energy emitted in the central thermal peak  $\xi < \xi_{min}$

$$L = \int (\rho/m_p)^2 \Lambda 4\pi r^2 dr = L_c \int_0^{\xi_{min}} \delta^2 \xi^2 d\xi \quad (21)$$

where

$$L_c = \left( \frac{3}{5} \right)^{1/2} \frac{1}{4\pi m_p^2} \frac{50}{(15 - 6a)} \frac{\dot{M}^2 \Lambda \theta_s^{1/2}}{GM}. \quad (22)$$

The asymptotic behavior of flow variables in the thermal peak as  $\xi \rightarrow 0$  is:  $\eta \propto \xi^{-1}$ ,  $\delta \propto \xi^{-3/2}$  and  $\tau \propto \xi^{-1}$ . Consequently, the integral for the total peak luminosity,  $\propto \int d\xi/\xi$ , diverges logarithmically at the origin. (If  $\Lambda$  had a bremsstrahlung temperature dependence  $\Lambda \propto T^{1/2}$ , the divergence would be even stronger.) Evidently this divergence is related to the concept of a point mass which can increase the internal energy and density of radially inflowing gas without limit. Obviously rotation, magnetic or relativistic effects must eventually alter the nature of idealized radiating Bondi flows within some radius, removing the apparent divergence of the luminosity  $L$  from the thermal peak.

In radiating Bondi flows having central thermal peaks the temperature in the peak increases as  $\tau \propto \xi^{-1}$  but the dimensionless entropy factor,  $\sigma = \tau/\delta^{2/3} \propto \xi^0$ , is constant and the radiative cooling time is longer than the flow time. Gas flows supersonically to the center along an adiabat. But this adiabat differs from that of classical adiabatic Bondi accretion for  $\gamma = 5/3$  in which gas flows subsonically toward the central point mass, becoming sonic as  $r \rightarrow r_s = 0$ . In our radiating flows the rapidly converging and accelerating central flow becomes effectively adiabatic for all values of  $a$  because of the short flow time, not because it stops radiating. Moreover, this central pseudo-adiabatic flow in  $r < r_s$  is entirely supersonic, unlike the subsonic central flow in classical Bondi flow.

The adiabatic character of asymptotic flow in central thermal peaks can be understood by comparing the two terms on the right in equation (3) that describe the importance of compression heating and radiation losses respectively. The ratio of thermal energy change due to radiation and compression is therefore

$$\sim \frac{\Lambda \dot{M}}{4\pi m_p^2} \cdot \frac{1}{\theta u^2 r} = \frac{3}{5} \cdot \frac{\Lambda \dot{M}}{4\pi m_p^2} \cdot \frac{1}{\theta_s^2 r_s} \cdot \frac{1}{\tau \eta \xi} \propto \xi.$$

While the luminosity due to cooling by radiative losses diverges as  $r \rightarrow 0$  during inflow in the thermal peak, the radiative term in equation (3) nevertheless becomes progressively smaller relative to the term for compressional heating which diverges even faster. As  $\xi \rightarrow 0$  the gas temperature is altered only by compression, explaining the adiabatic nature of the flow inside the central thermal peak.

### 3.1. Cooling Site Flows

Cooling site solutions in which  $M \rightarrow 0$  are a well defined limit of radiating Bondi flows. In this limit  $a \rightarrow -\infty$  while  $\dot{M}$  and  $\Lambda$  remain finite. Flows for large  $|a|$  in Figure 1 remain essentially unchanged for  $|a| \geq 100$ , so the  $|a| = 100$  profiles can be regarded as essentially equivalent to the (non-gravitating) cooling site flow. In cooling site flow the gas cools completely at some finite radius  $\xi_{cool} < 1$  where all its entropy  $\sigma = \tau/\delta^{2/3}$  is radiated away. In these flows the total radiated emission within the sonic radius

$$L \approx L_c \log(1/\xi_{cool})$$

is finite.

## 4. CONFRONTING OBSERVATIONS

Of interest are potential sources of error when accretion rates are estimated by calibration with radiating and non-radiating Bondi flows. For this purpose it is necessary to convert from dimensionless to physical variables.

#### 4.1. Classical Bondi Flows

In traditional Bondi accretion with  $\gamma = 5/3$  gas flows with constant entropy toward a mass point at the origin. Very far from the mass point the gas is at rest with uniform density  $\rho_\infty$  and temperature or sound speed  $c_\infty$ , that define the adiabat for the entire flow. However, in Bondi solutions for a typical monatomic gas with  $\gamma = 5/3$  the only flow from large radii to the origin must be fully subsonic, reaching the sound speed just at the origin,  $r_s = 0$ . When  $\gamma = 5/3$  the energy integral for the steady flow is

$$\frac{1}{2}u^2 + \frac{3}{2}c_s^2 - \frac{GM}{r} = \frac{1}{2}u_\infty^2 + \frac{3}{2}c_\infty^2. \quad (23)$$

If the gas velocity  $u_\infty$  vanishes as  $r \rightarrow \infty$ , the Bondi accretion rate is

$$\dot{M} = \pi(GM)^2 \frac{\rho_\infty}{c_\infty^3} \quad (24)$$

where the coefficient  $\rho_\infty/c_\infty^3$  is related to the inverse of the entropy factor,  $c_\infty^3/\rho_\infty \propto (T/\rho^{2/3})^{3/2}$ . For a fixed central mass the accretion rate decreases with increasing gas entropy. When estimating the classical quadratic Bondi dependence,  $\dot{M} \propto M^2$ , the entropy factor  $c_\infty^3/\rho_\infty$  in equation (24) is assumed to be independent of  $M$ . But it is easy to imagine astronomical correlations between entropy and  $M$  that are unrelated to the hydrodynamics: larger black hole masses are often found at the centers of more massive dark halos containing gas with higher entropy.

The Bondi accretion rate  $\dot{M}$  onto galaxy or cluster-centered black holes can be estimated from X-ray observations of gas temperature and density profiles. Gas observed at some radius just larger than  $\sim GM/c_s^2$ , where the black hole potential begins to dominate, is assumed to be essentially at rest. For example, Allen et al. (2006) estimated  $\rho_A$  and  $T_A$  from (inward extrapolated) observations at radius  $r_A = GM/2c_A^2$  where  $c_A = (\gamma k T_A / \mu m_p)^{1/2}$  is the local sound speed at  $r_A$  and  $M$  is known from observations of the central galaxy. Since the entropy factor  $c_s^3/\rho$  is constant in Bondi flow, it can be observed at any radius. However, the Bondi flow morphology and equation (24) require  $u_\infty = 0$ .

#### 4.2. Radiating Bondi Flows

In radiating Bondi flows radiation losses occur at all radii so the flow at large distances from the gravitating mass point necessarily has gradients unlike the traditional Bondi flow. For  $\xi \gtrsim 100$ ,  $d \log \eta / d \log \xi = -2$  and  $d \log \tau / d \log \xi = 1$  are excellent approximations to radiating solutions in Figure 1 when  $\xi \gtrsim \xi_{min}$ . Consequently, the sound speed and gas density at infinity are not defined nor is this limit relevant in comparing with observation.

Radiating accretion flows are inherently non-adiabatic. However, for  $|a| \lesssim 1.5$  radiating supersonic Bondi flows ultimately become adiabatic as  $\xi \rightarrow 0$  in the central ther-

mal peak, having passed through a temperature minimum and a sonic point. The sonic radius,

$$r_s = 13 \frac{(15 - 6a)}{21} \frac{(M/10^9 M_\odot)}{(T_s/10^7 \text{K})} \text{ pc} \quad (25)$$

is likely to be small, not directly observable. Remarkably, the morphology of all radiating Bondi flows is determined by a single dimensionless parameter  $a$ . The accretion rate is

$$\dot{M} = a \cdot 4\pi m_p^2 \frac{3c_s^2}{5} \frac{GM}{\Lambda} \quad (26)$$

where  $c_s = u_s$  is the sound speed at the sonic radius.

Alternatively, by using equation (19) the radiating accretion rate can be written in terms of the sonic radius

$$\dot{M} = a \cdot 4\pi m_p^2 \frac{GM}{\Lambda} \left( \frac{15 - 6a}{50} \right) \frac{GM}{r_s}. \quad (27)$$

While the quadratic mass dependence in this less useful representation  $\dot{M} \propto M^2$  resembles the classical Bondi relation, its coefficient  $a(15 - 6a)/r_s$  cannot be directly observed and has a complex dependence on the flow variables.

Flows having the same  $\dot{M}/M$  and  $T_s$  (and therefore  $a$ ) have identical temperature and density profiles  $T(r)$  and  $\rho(r)$  and for these flows the linear relation  $\dot{M} \propto M$  holds exactly. However, the relation  $\dot{M} \propto a M c_s^2$  from equation (26) does not in general imply that  $\dot{M} \propto M^p$  with  $p = 1$ , nor does it imply that  $\dot{M}$  and  $M$  are necessarily related with a simple power law. While accretion flows expressed in dimensionless variables, as in Figure 1, depend on the single parameter  $a$ , the same flows translated into dimensional variables  $u(r)$ ,  $T(r)$  and  $\rho(r)$  depend on any two of the parameters  $a$ ,  $M$  and  $T_s$ , assuming that  $M$  is independently known from observations of the central galaxy.

A more general relationship between  $\dot{M}$  and  $M$  can be established by considering intersecting flows. In particular, by varying  $\dot{M}$  and  $T_s$  it is possible to construct radiating flows having different central masses  $M$  that share the same temperature  $T$  and density  $n_e = \rho/(1.17m_p)$  at the same radius  $r$ . Such intersecting flows have different  $a$  and different morphologies. For example, Figure 2 shows three radiating Bondi flows that intersect with identical gas properties. Only the subsonic regions of these flows are plotted, extending from the sonic radius  $r_s$  at the left to 1 kpc at the right. The solid line profile is a reference solution with parameters  $M = 3 \times 10^9 M_\odot$ ,  $\dot{M} = 0.3 M_\odot \text{ yr}^{-1}$ , and  $T_s = 3 \times 10^6 \text{ K}$ . The dashed lines are two radiating Bondi flows with lower central mass  $M/3$  that intersect the reference flow at points 1 and 2 where they have the same  $T$  and  $n_e$  at  $r_1$  and  $r_2$ . The upper dashed flow profiles  $(M/3)_1$  in both panels of Figure 2 intersect at  $r_1 = 152.2 \text{ pc}$  (point 1) where  $T = 2.21 \times 10^6 \text{ K}$  and  $n_e = 0.182 \text{ cm}^{-3}$ . The parameters of this flow are  $M = 10^9 M_\odot$ ,  $\dot{M} = 0.07917 M_\odot \text{ yr}^{-1}$ , and  $T_s = 1.76 \times 10^7 \text{ K}$ . The lower dashed flow profiles  $(M/3)_2$  in Figure 2, based on parameters  $M = 10^9 M_\odot$ ,  $\dot{M} = 0.17929 M_\odot \text{ yr}^{-1}$ , and  $T_s = 9.00 \times 10^5 \text{ K}$ , intersect at  $r = 624.3 \text{ pc}$  (point 2) where  $T = 1.432 \times 10^6 \text{ K}$  and  $n_e = 0.03568 \text{ cm}^{-3}$ .

Of interest are the differing values of  $\dot{M}$  and  $M$  for the two flows involved at each of these intersections and in particular the mean power law variation  $\dot{M} \propto M^p$  that approximately describes how the accretion rate varies with central mass for flows with central masses in the range  $M/3 - M$ , all of which intersect with the reference solution at the same point. From the two very specific intersections shown in Figure 2 at points 1 and 2 we find that  $\dot{M} \propto M^p$  with  $p = 1.21$  and  $0.47$  respectively. The exponent  $p$  differs from unity because the three intersecting flows in Figure 2 have different overall morphologies and values of  $a$ . The three flows in the upper panel of Figure 2 can be ordered  $-(M/3)_1, M, (M/3)_2$  - with decreasing  $r_{min}/r_s$  where  $r_{min}$  is the radius of minimum gas temperature and the sonic radius  $r_s$  is defined by the leftmost extent of each flow. A qualitatively similar morphological sequence for decreasing  $r_{min}/r_s = \xi_{min}$  is apparent in the central panel of Figure 1 for flows with  $|a| = 0.01, 0.1$  and  $1$ . This is consistent with similarly increasing values of  $|a| = 0.0137, 0.1008$  and  $0.6027$  respectively that characterize the intersecting flows  $(M/3)_1, M$ , and  $(M/3)_2$  in Figure 2.

The dotted lines  $(2M/3)_1$  in Figure 2 show a third root through point 1 with parameters:  $2M/3 = 2 \times 10^9 M_\odot$ ,  $\dot{M} = 0.1725 M_\odot \text{ yr}^{-1}$ ,  $T_s = 9.3 \times 10^6 \text{ K}$  and  $|a| = 0.02806$ . The variation of  $p$  between the three roots is not constant:  $p = 1.12$  for  $(M/3)_1 \rightarrow (2M/3)_1$  and  $p = 1.36$  for  $(2M/3)_1 \rightarrow M$ . Evidently, there is no general power law relation  $\dot{M} \propto M^p$  that applies to all intersecting flows of this type, although local values of  $p$  are not far from unity.

Also clear from Figure 2 is that the mass accretion rate  $\dot{M}$  cannot be determined by observations of  $T$  and  $n_e$  at a single radius. The parameters of radiating flows,  $\dot{M}$  and  $T_s$ , must be found with fits to a spatially extended set of observations that extend close to or within the radius of minimum temperature. The best-fitting flow parameters  $\dot{M}$  and  $T_s$  can be found with iterative integrations out from the sonic radius as we have done here.

Three additional points: (1) Although we consider intersecting accretion flows having different  $M$  to explore the  $\dot{M} \propto M^p$  relation, it must be stressed that not all flow solutions intersect nor do they intersect as shown in Figure 2. For example, subsonic entropy factor profiles  $S(r) = T(r)/n_e^{2/3}(r)$  do not intersect when only the sonic temperature  $T_s$  is varied. Subsonic entropy profiles in which only  $\dot{M}$  varies typically intersect but, unlike Figure 2, the values of  $T$  and  $n_e$  are not identical at intersections having the same entropy  $T/n_e^{2/3}$ . The unusual flow intersections in Figure 2 with identical  $T$  and  $n_e$  but varying mass  $M$ ,  $T_s$  and  $\dot{M}$  reveal a relationship between  $a = a(T_s, \dot{M}/M)$  and the exponent  $p$ . Unlike traditional Bondi flows, the  $\dot{M}(M)$  relation for radiating Bondi flows is not defined by the entropy  $T/n_e^{2/3}$  at a single radius of observation. (2) When  $\dot{M}$  is known in advance, the morphology parameter depends on the sonic temperature and accretion rate,  $a = a(T_s, \dot{M})$ . As  $T_s$  and  $\dot{M}$  are varied to match observations of a single flow or when a group of similar flows are compared, the range of  $T_s$  and  $\dot{M}$  for successful fits is limited and correspond to a relatively small variation in  $a$ . When  $M$  and  $\dot{M}$  are

compared among these flows, we expect  $p \approx 1$ . (3) We draw attention to the relative insensitivity of the index  $p$  to the morphology parameter  $a$  in the intersecting examples illustrated in Figure 2. As  $|a|$  increases from  $0.0137$  to  $0.6027$ , a factor of  $44$ ,  $p$  changes only from  $1.21$  to  $0.47$ . In addition, for massive galaxy-centered black holes  $a$  is constrained by observations:  $|a| \lesssim 3$  is required to avoid total off-center cooling (eqn 28) which is not generally observed and  $|a|$  cannot be very much less than  $0.01$  since temperature minima are rarely observed at large radii. This also suggests that  $p$  lies in a restricted region near unity.

In Figure 3 we compare the accretion rate for the reference solution  $\dot{M} = 0.3 M_\odot \text{ yr}^{-1}$  with estimates of  $\dot{M}$  using the classical Bondi procedure (eqn 24). The Bondi mass flow rates  $\dot{M}$  are determined from flow local gas temperature and density of the reference solution. It is seen that the classical Bondi solution considerably underestimates  $\dot{M}$  in the region plotted. The decreasing classical Bondi  $\dot{M}$  with radius mirrors the monotonically increasing entropy in the radiating solution.

Equation (24) for Bondi flow is used extensively in computations of cosmological black hole accretion (e.g. Springel et al. 2005; Johansson et al. 2009; Dubois et al. 2010; Kim et al. 2011). But successful black hole growth is only possible if the Bondi accretion rate is enhanced by a large *ad hoc* dimensionless coefficient, while such a factor  $a$  appears naturally in radiating Bondi flows (eqn 26). Bondi accretion is also invoked to estimate accretion rates  $\dot{M}$  from X-ray observations of hot gas surrounding galaxy-centered and cluster-centered black holes (e.g. Allen et al. 2006; Balmaverde et al. 2008; Vattakunnel et al. 2010). However, as with the cosmological computations, X-ray observations of sources having greater feedback power require mass accretion rates considerably in excess of the Bondi rate (Rafferty et al. 2006; Hardcastle et al. 2007; McNamara et al. 2011). In addition to the large mass accretion rates implied by radiative emission from luminous black holes in AGNs and quasars, a comparable accretion rate is required to provide the huge mechanical power expended by cluster-centered black holes in expanding the cluster gas to match observed gas mass fraction profiles (Mathews & Guo 2011).

In radiating Bondi flows the temperature dependence in this outer region  $\xi > \xi_{min}$ ,  $\tau \propto \xi$ , is a reasonable match to gas temperature profiles in the central region of most galaxy groups and clusters. Moreover, the density in  $\xi > \xi_{min}$  varies asymptotically as  $\delta \propto \xi^{-1/2}$  so the entropy is not constant but varies rather significantly with radius,  $\sigma = \tau/\delta^{2/3} \propto \xi^{4/3}$ , at large  $\xi$  in radiating Bondi flows. However, hot gas observed in more isolated elliptical galaxies can have  $dT/dr < 0$ . This can be understood if the gas is confined by a halo of lower mass (Humphrey et al. 2006) or, at smaller radii, by compressional heating near the central black hole (Humphrey et al. 2008).

Positive temperature gradients typically observed on kpc scales in galaxy groups and clusters are evidently imposed by entropy-losing cooling flows in the gravitational potential of the stars and the group/cluster dark matter on larger multi-kpc scales. These flows on larger scales have local enclosed masses greatly exceeding that

of the central black hole and contain gas with a larger virial temperature. Consequently, the gas flow rate  $\dot{M}$  toward cluster-centered black holes depends not just on the black hole mass but on the huge mass of baryonic gas bound to the dark halo of the surrounding galaxy group or cluster. These large scale temperature and density gradients further confound estimates of the black hole accretion rate using the traditional Bondi recipe (eqn 24). Once the innermost resolvable (or extrapolated) gas density and temperature are interpreted as  $\rho_\infty$  and  $T_\infty$ , the Bondi formula provides a unique local value of  $\dot{M} = \pi(GM)^2\rho_\infty/c_\infty^3$  for each  $M$ . By contrast, the corresponding relation for radiating Bondi flows,  $\dot{M} \propto aMT_s$ , contains the additional dimensionless parameter  $a$  that can be adjusted to fit much larger mass flows  $\dot{M}$  that approach the central black hole from radiating gas bound to the surrounding group or cluster halos.

Large values of the parameter  $|a|$  can be regarded as a measure of large accretion rates that may cool significantly before reaching the central black hole. According to Figure 1, off-center cooling requires  $|a| \gtrsim 3$  which, with equation (26), corresponds to larger accretion rates

$$|\dot{M}| \gtrsim 30 \left( \frac{\Lambda}{10^{-23} \text{erg cm}^3 \text{s}^{-1}} \right)^{-1} \frac{T_s}{10^7 \text{K}} \frac{M}{10^9 M_\odot} \frac{M_\odot}{\text{yr}}. \quad (28)$$

This is roughly consistent with observations of significant central star-formation in many X-ray luminous cool-core clusters (e.g. Donahue et al. 2010), although this occurs on scales larger than the sonic radius for the black hole. This inequality also expresses a bimodality between hot ( $|a| \lesssim 3$ ;  $|\dot{M}| \lesssim 30 M_\odot \text{ yr}^{-1}$ ) and cold ( $|a| \gtrsim 3$ ;  $|\dot{M}| \gtrsim 30$ ) modes of accretion by central black holes. Radiating accretion flows that cool before reaching the central mass are those with small central mass  $M$ , lower temperature, or, as in the example above, large accretion rates  $\dot{M}$  (Sarazin & White 1987; Quataert & Narayan 2000).

## 5. CONCLUSIONS

Gas flowing near accreting black holes can only be observed with radiation that necessarily carries entropy

away from the flow, in violation of the adiabatic assumption inherent in traditional Bondi flows. However, when radiative cooling is included, the accretion flow solutions are qualitatively different, not merely perturbations or limiting cases of the original Bondi flow. Nevertheless, radiating solutions have widely varying morphologies that depend on a single dimensionless parameter and they all must pass through a sonic point. Although the gas density (entropy) decreases (increases) monotonically with radius, many solutions exhibit a broad temperature minimum. Far from the mass point the temperature and entropy increase, allowing fits to be made to gas flowing subsonically in from a deeper potential well having a larger virial temperature. Some radiating accretion flows do not pass through a temperature minimum, but instead cool completely before reaching the central mass. In ‘‘cooling site’’ flows, in which there is no central mass, total cooling occurs at a non-zero radius within the sonic point.

Of particular interest is the failure of traditional Bondi flows to accurately relate the mass accretion rate to the central mass. The traditional Bondi result  $\dot{M} \propto M^p$  with  $p = 2$  is certainly incorrect for radiating flows. The examples we consider indicate much smaller values  $p \sim 1$  in which the precise value of  $p$  is somewhat sensitive to the flow morphology.

The idealized radiating Bondi flow we describe here, while certainly an improvement over the classic adiabatic Bondi flow, cannot be valid within some radius. Any small rotation in the initial gas must ultimately flow into a disk. Nevertheless, these idealized spherical radiating solutions may provide a useful framework for understanding more realistic flows that include rotation, magnetic fields, viscosity, feedback, etc. They may also be useful in evaluating the performance of central or non-central cooling in numerical computations.

Our colleague Fabrizio Brighenti provided helpful advice. We also acknowledge with thanks insights provided by the referee who challenged us to provide explicit examples of non-quadratic relations between  $\dot{M}$  and  $M$ . Studies of feedback gasdynamics in hot intracluster gas at UC Santa Cruz are supported by NSF and NASA grants for which we are very grateful.

## REFERENCES

- Allen, S. W., Dunn, R. J. H., Fabian, A. C., Taylor, G. B., Reynolds, C. S. 2006, MNRAS 372, 21
- Balmaverde, B., Baldi, R. D., & Capetti, A. 2008, A&A, 486, 119
- Bondi, H., 1952, MNRAS 112, 195
- Brighenti, Fabrizio; Mathews, William G.; Humphrey, Philip J.; Buote, David A., 2009, ApJ, 705, 1672
- Cowie, L. L. & Binney, J. 1977, ApJ, 215, 723
- Donahue, M. et al. 2010, ApJ, 715, 881
- Dubois, Y., Devriendt, J., Slyz, A., & Teyssier, R., 2010, MNRAS 409, 985
- Fabian, A. C. & Nulsen, P. E. J. 1977, MNRAS, 180, 479
- Guo, F., Oh, S. P. & Ruszkowski, M. 2008, ApJ, 688, 859
- Johansson, P. H., Naab, T., & Burkert, A. 2009, ApJ, 690, 802
- Hardcastle, M. J., Evans, D. A., & Croston, J. H. 2007, MNRAS, 376, 1849
- Humphrey, P. J., Buote, D. A., Brighenti, F., Gebhardt, K., Mathews, W. G. 2008, ApJ, 683, 161
- Humphrey, P. J., Buote, D. A., Gastaldello, F., Zappacosta, L., Bullock, J. S., Brighenti, F., & Mathews, W. G. 2006, ApJ, 646, 899
- Kim, J., Wise, J. H., Alvarez, M. A., & Abel, T. 2011, ApJ, 738, 54
- Mathews, W. G. & Guo, F. 2011, ApJ, 738, 155
- Mathews, W. G. & Bregman, J. N. 1978, ApJ, 224, 308
- McNamara, B. R., Rohanizadegan, M. & Nulsen, P. E. J. 2011, ApJ, 727, 39
- Narayan, R. & Fabian, A. C. 2011, MNRAS, 415, 3721
- Park, M.-G. 2009, ApJ, 706, 637
- Quataert, E. & Narayan, R. 2000, ApJ 528, 236
- Rafferty, D. A., McNamara, B. R., Nulsen, P. E. J., & Wise, M. W. 2006, ApJ, 652, 216
- Sarazin, C. L. & White, R. E., III, 1987, ApJ, 320, 32
- Springel, V., Di Matteo, T., & Hernquist, L. 2005, MNRAS, 361, 776
- Sutherland, R. S. & Dopita, M. A. 1993, ApJS 88, 253
- Vattakunnel, S., Trussoni, E., Capetti, A., & Baldi, R. D. 2010, A&A, 522, A89
- Yahil, A. & Ostriker, J. P. 1973, ApJ, 185, 787

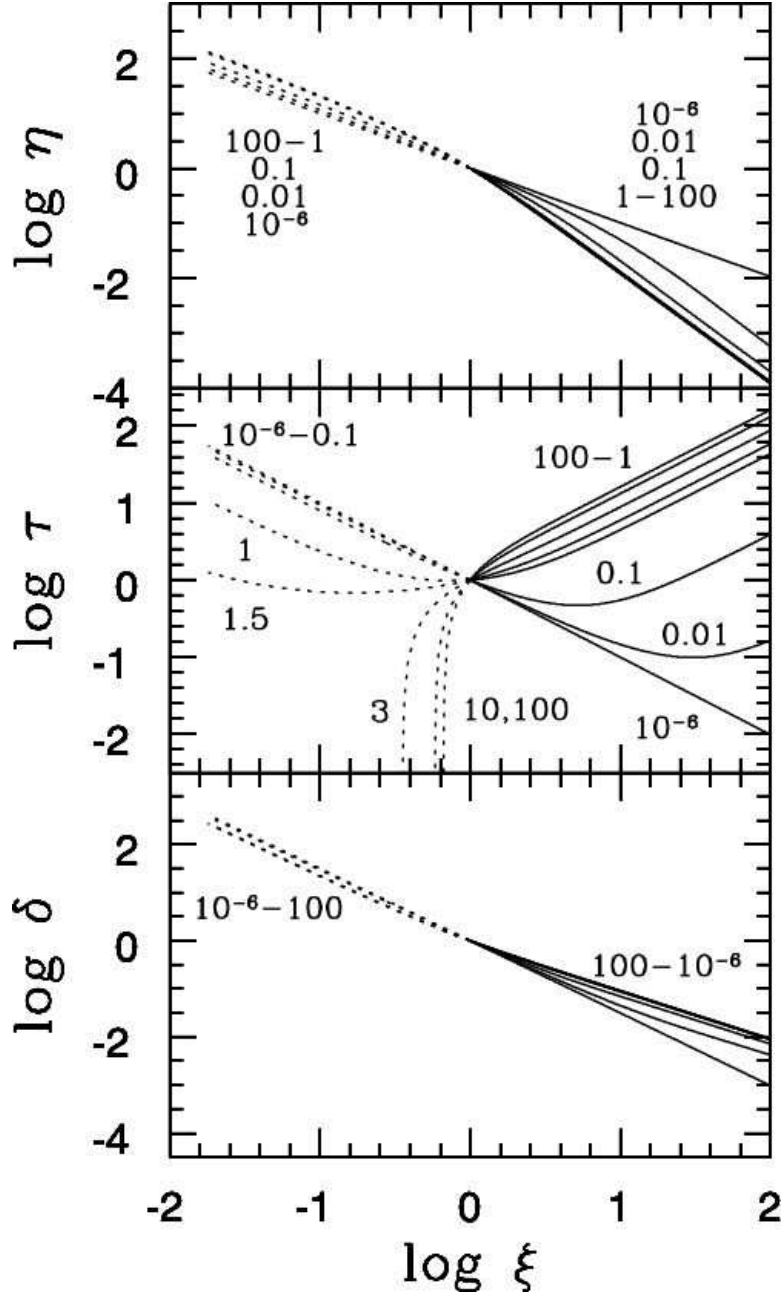


FIG. 1.— Plot of radiating Bondi flows in dimensionless variables. *Top:* Dimensionless (square of the) velocity  $\eta(\xi)$ . *Center:* Dimensionless temperature  $\tau(\xi)$ . *Bottom:* Dimensionless density  $\delta(\xi)$ . Where possible, each curve is labeled with its dimensionless parameter  $|a|$ . Profiles that are too crowded to label individually are identified with the range in  $|a|$  in order of decreasing variable  $\eta$ ,  $\tau$  or  $\delta$ .

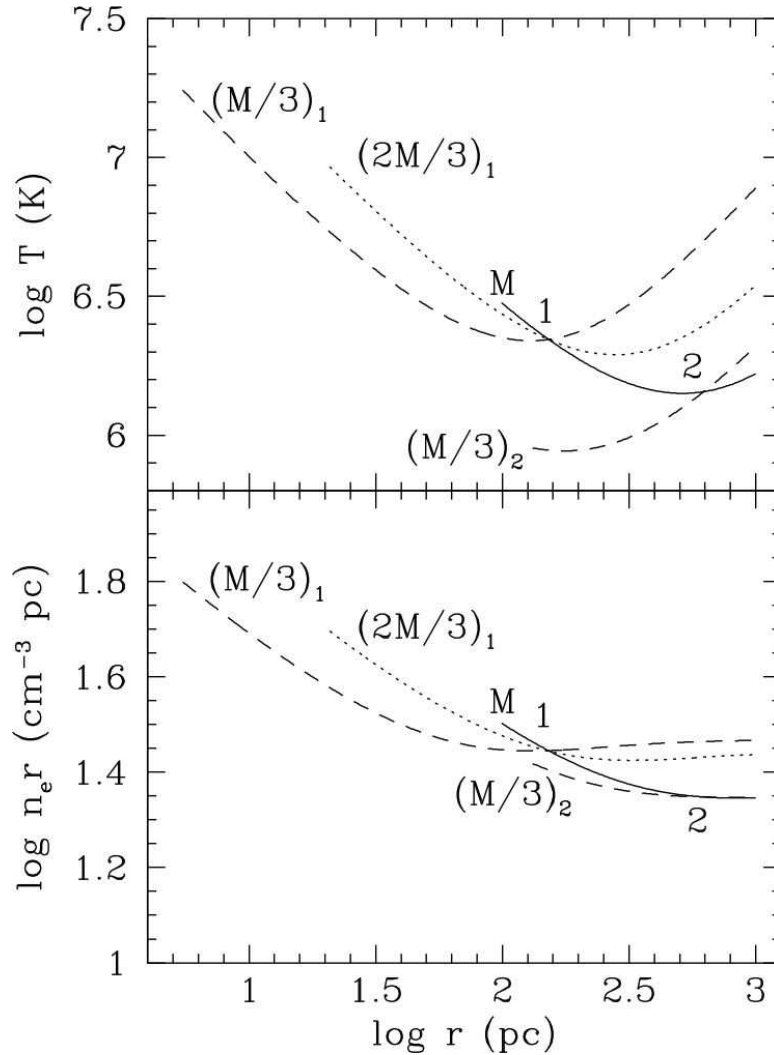


FIG. 2.— *Upper* and *Lower* panels show respectively gas temperature and density profiles of the subsonic regions of three radiating accretion flows, each extending from 1 kpc at the right to the sonic radius  $r_s$  at the left. For better visibility the gas density is multiplied by the radius in the lower panel. Solid lines show a reference solution for which  $M = 3 \times 10^9 M_\odot$ ,  $\dot{M} = 0.3 M_\odot \text{ yr}^{-1}$ , and  $T_s = 3 \times 10^6$  K. The dashed lines show two additional flows  $(M/3)_1$  and  $(M/3)_2$  for which the black hole mass  $M = 10^9 M_\odot$  is three times smaller. Parameters  $\dot{M}$  and  $T_s$  for the two dashed profiles have been chosen so that the intersections with the reference flow at points 1 and 2 at radius  $r$  have the same temperature and density as the reference solution. The dotted lines  $(2M/3)_1$  show a third root through point 1 for an intermediate mass. The objective is to explore how  $\dot{M}$  varies with  $M$  for flows observed having identical  $T$  and  $n_e$  at some radius.



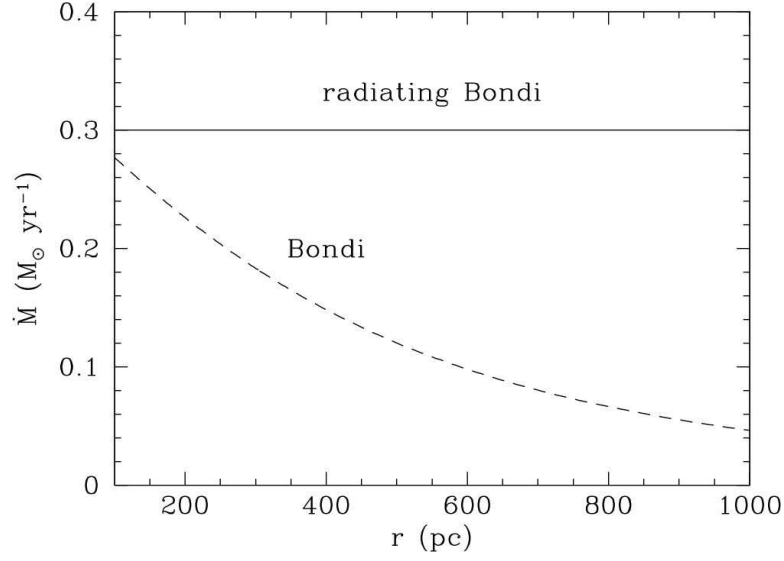


FIG. 3.— The solid line shows the constant mass accretion profile  $\dot{M} = 0.3$  for the reference radiating Bondi solution for  $M = 3 \times 10^9 M_{\odot}$ ,  $\dot{M} = 0.3 M_{\odot}$ , and  $T_s = 3 \times 10^6$  K. The dashed line shows the mass accretion rate for classic Bondi flows estimated with  $\dot{M} = \pi(GM)^2 \rho_{\infty} / c_{\infty}^3$  with the usual assumption  $\rho_{\infty} = \rho(r)$  and  $c_{\infty} = c_s(r)$ .